International Journal of
Automotive Manufacturing and Materials（IJAMM）

Scilight

Article

Design and Optimization Analysis of Combustion Chamber for Equivalent Ratio Combustion Gas Engine

Huan Chen *, Zhi Li, Bei Liu, Huiya Zhang, Qinya Zhang, Feifei Gou, and Hongfei Zhang

Dongfeng Commercial Vehicle Technical Center, Dongfeng Motor Co. Ltd., Wuhan 430056, China
* Correspondence: yf-chenhuan@dfcv.com.cn
Received: 24 March 2025; Revised: 9 April 2025; Accepted: 23 July 2025; Published: 4 August 2025

Abstract: Four types of combustion chambers, including constricted type, shallow pit, flat top, and spherical, were proposed for the equivalence ratio combustion gas engines, and relevant calculations were conducted to explore the combustion characteristics. The results show that the deep pit type shows good flow characteristics, such as high Turbulent Kinetic Energy (TKE) and high tumble flow, exhibiting quick flame spread and excellent combustion characteristics; The constricted combustion chamber generates TKE and rolling flow near the spark plug, resulting in a poor flame formation process. Meanwhile, the low compression height reveals the poor flame propagation towards the periphery of the combustion chamber; The spherical combustion chamber performs well in the flame formation and development cause of rolling flow and TKE generation near the spark plug, However, due to wall interactions, the flame propagation process is relatively poor; Overall, the balance between compression height and combustion chamber depth must be considered in combustion design to optimize the in cylinder flow and combustion characteristics of the engine.

Keywords: gas engine; combustion chamber; flow characteristics; combustion characteristics

1. Introduction

Natural gas as a clean fuel has been forced to be the mainstream energy in the engine industry to comply with the increasingly strict emission regulations. However, Natural gas engines are constrained by slow combustion speed, long combustion duration, and detonation, resulting in low thermal power conversion efficiency, high cylinder heat load, high exhaust temperature, and large combustion cycle fluctuations. Reducing heat load and achieving better engine performance contribute to accelerating the combustion rate, so that the performance of natural gas engines can be improved.

Computational research on the design of combustion chambers for spark ignition engines was conducted extensively. A multidimensional model was used by Jin Kusak [1] to analyze the effect of premixed gas concentration on combustion. The results indicate that the high concentration of natural gas can improve combustion and reduce THC and CO emissions due to the fast consumption rate of premixed gas and high cylinder gas temperature. Qingping Zheng from Tianjin University [2] used AVL-FIRE software to analyze the effects of combustion chamber structural parameters on ignition timing, average cylinder temperature and pressure, and NO emissions in a partitioned compression ignition natural gas engine. Shinichi Goto [3] surveyed the influence of combustion chambers on the combustion and performance of lean-burn LPG engines. Gulcan et al. [4] revealed that a toroidal re-entry combustion chamber (TRCC) design in methane-diesel dual-fuel engines contributes to more complete combustion and lower emissions. Bao et al. [5] mathematically analyzed the combustion characteristics, engine performance, and pollutant emissions of various piston bowl designs in natural gas engines. Xu et al. [6] optimized the piston bowl geometry and fuel injection strategy based on the dual-mode dual-fuel (DMDF) combustion concept, thereby enhancing thermal efficiency across the entire load range. Li et al. [7] noted that the combination of an eccentric hemispherical

combustion chamber (EHCC) and a mixed-flow intake port achieves an effective thermal efficiency of over 41.53%.

Protrusions on the piston crown oriented toward the combustion chamber can shatter large-scale vortices, augmenting the cylinder average turbulent kinetic energy during the main combustion phase [8]. Alternatively, the squeeze flow generated by the piston crown can disrupt the cylinder's large-scale vortices [9]. Fu [10] designed six combustion chamber configurations for a heavy-duty natural gas engine, revealed that a higher heat release rate was correlated with the larger volume occupied by high-turbulence kinetic energy regions, and highlighted the importance of optimizing the combustion chamber in regulating the proportion and duration of high-turbulence kinetic energy regions within the cylinder. Zhang et al. [11] emphasized that optimized combustion chamber designs in natural gas engines enhance lean burn efficiency. Higher turbulence within chambers boosts combustion speed, aiding flame kernel formation and propagation. However, the elevated temperatures from faster flame propagation can increase NOx emissions. Evans et al. [12] developed a combustion chamber featuring enhanced squeeze flow, which increased in-cylinder turbulence, improved engine stability, and decreased specific fuel consumption by 4.8%.

Despite extensive research on natural gas engines, their application in heavy-duty commercial vehicles remains immature [13,14]. To fill this research gap, this study focuses on a 13 L displacement natural gas engine and proposes four combustion chamber schemes. These schemes aim to seek the balance between compression height and combustion chamber depth, and to achieve the synergistic optimization of turbulence characteristics and combustion rate [15,16]. This approach extends beyond traditional optimization methods that focus solely on combustion chamber shape or a single performance metric [17].

A new three-dimensional numerical simulation method was established to study the influence of combustion chamber design on the in-cylinder flow and combustion characteristics of natural gas engines. The differences in in-cylinder flow and combustion characteristics among the four types of combustion chambers were analyzed and compared, and several conclusions regarding natural gas engine combustion chamber design were summarized to provide innovative insights and references for the optimization of combustion chamber design.

2. Establishment of Simulation Calculation Model

2.1. Engine Structural Parameters

A natural gas engine based on a 6-cylinder diesel engine, with a displacement of 13 L, is modeled. The equivalence ratio + EGR and spark plug center ignition are adopted. The structural parameters of the engine are shown in Table 1.

Table 1. Engine Structural Parameters.

Number	Parameter	Unit	Value
1	Stroke	/	4
2	cylinders	/	6
3	Cylinder arrangement	/	inline
4	Cylinder diameter	mm	131
5	Stroke	mm	160
6	Connecting rod length	mm	265

2.2. Calculation Conditions

The impact of combustion chamber design on combustion and performance is discussed without considering the influence of operating conditions. Comparative calculations are conducted based on fixed operating conditions. In addition, the mixing process of natural gas, air, and EGR is not considered in the calculation process. Simulation Calculation Conditions and Parameters are listed in Table 2.

Table 2. Simulation Calculation Conditions and Parameters.

Number	Parameter	Unit	Value
1	Engine speed	r/min	1800
2	Engine load	%	100
3	Compression ratio	-	11.5
4	Air-fuel ratio	-	21.23:1
5	EGR rate	%	19
6	Ignition timing	°CA	−32

2.3. Calculation Model

Established engine combustion calculation model based on Converge software includes cylinder head, cylinder block, cylinder gasket, spark plug, cylinder liner, valve gasket, valve guide, valve, intake and exhaust passages, as shown in Figure 1. Notably, the mesh around the spark plugs and boundary areas is minimized while ensuring accuracy, so that computational workload can be alleviated.

2.4. Boundary Conditions

The transient simulation of an engine cycle for each combustion chamber is performed, with the engine operating at 1800 rpm and the throttle fully open; The cylinder simulation starts from the opening of the exhaust valve and ends after ignition at top dead center (TDC); The total pressure inlet and static pressure outlet boundary conditions are applied to the inlet and outlet respectively, as shown in Figure 2; among which Figure 2a shows Schematic diagrams of the inlet and outlet, Figure 2b shows pressure boundary condition and Inlet temperature. The temperature of the inlet fluid is used as the input for simulation, and the exhaust temperature is calculated by the model; The isothermal boundary conditions are given for each surface in the model, as shown in Table 3.

2.5. Model Calibration and Grid-Independence Verification

The model calibration is divided into two stages: the pure compression stage and the ignition combustion stage. The pure compression section contains the period from the end of inhalation to the ignition stage. The ignition combustion section covers the stages from ignition to the end of combustion. The model calibration results are shown in Figure 3. The cylinder pressure curves of the experiment and simulation match well, with an error of within 5%, indicating that the model can reflect the physical and chemical processes of the cylinder accurately.

In 3-D simulations, reasonable meshing simultaneously guarantees numerical accuracy and minimizes computational expense. Grid independence, therefore, mandates systematic sensitivity analyses of both base and minimum grid sizes.

Structured grids with edge lengths of 4, 3, 2, and 1 mm were evaluated. The simulation results show that the 2 mm and 1 mm curves are nearly congruent, differing by 1.2% in peak pressure with identical crank-angle phasing. Additional refinement exerts negligible influence, so a 2 mm base mesh was adopted.

An adaptive strategy, driven by temperature and velocity gradients, refines the 2 mm base grid to minimum cells of 1, 0.5, 0.25, and 0.125 mm. The computational results reveal that further reduction from 0.25 mm to 0.125 mm yields only a 1.3% peak-pressure change while CPU time escalates markedly; hence, 0.25 mm was selected.

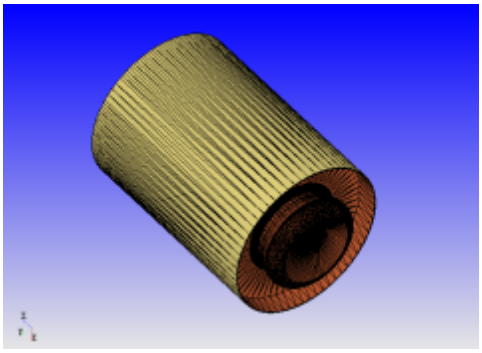

(a) Cylinder model.

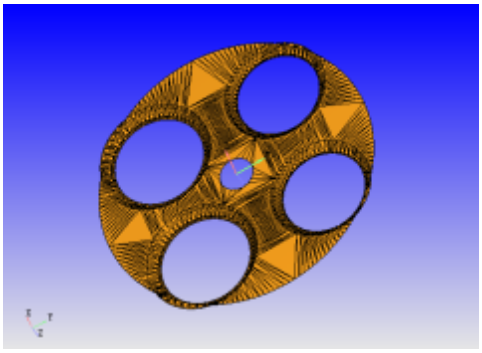

(b) Cylinder head bottom model.

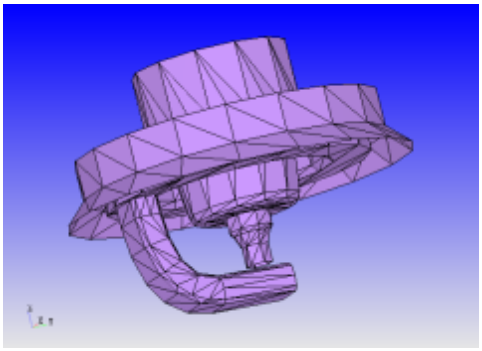

(c) Spark plug model.

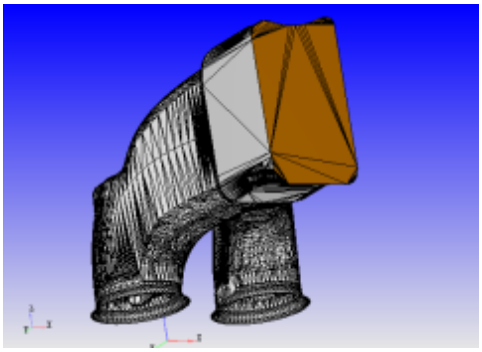

(d) Inlet port model.

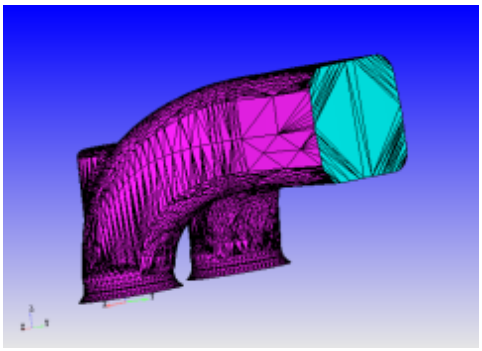

(e) Exhaust port model.

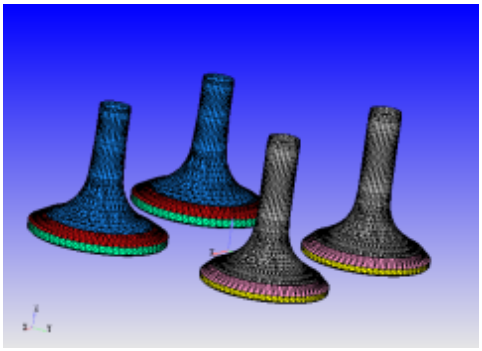

(f) Air valve model.

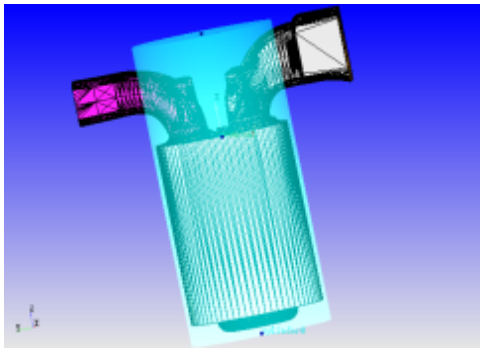

(g) Overall Model.

Figure 1. Combustion Calculation Model.

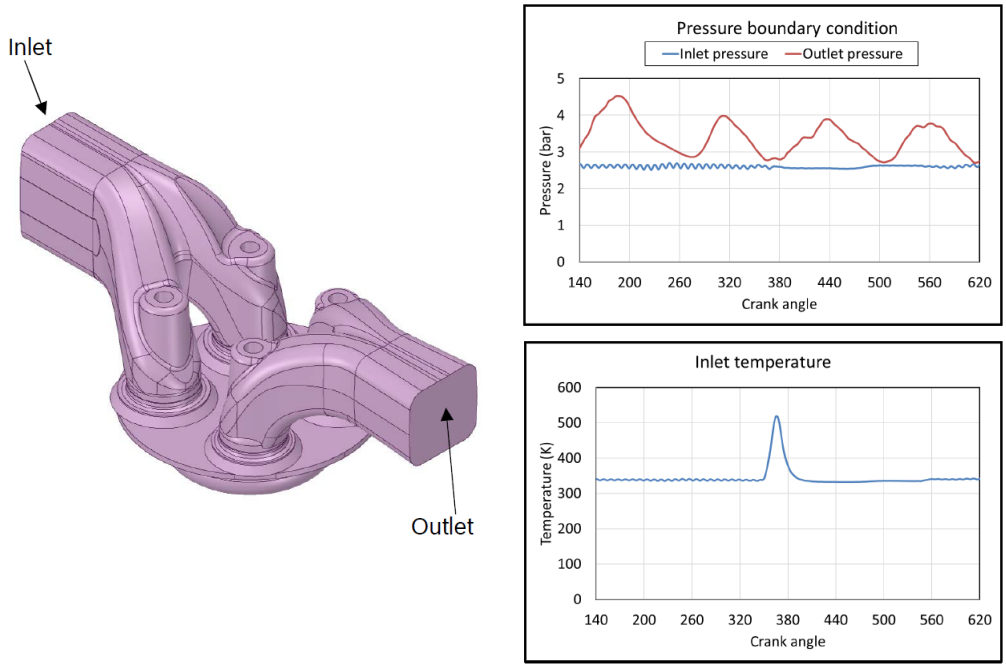

(a) Schematic of the inlet and outlet. **(b)** pressure boundary condition and Inlet temperature.

Figure 2. Boundary conditions for inlet and outlet pressure and temperature.

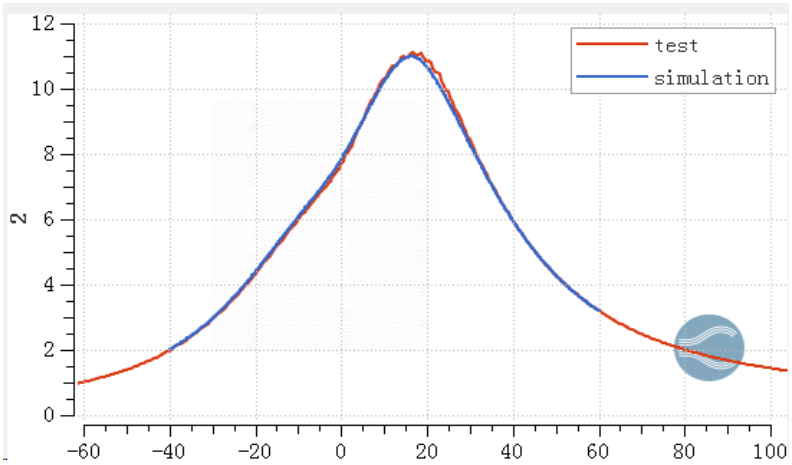

Figure 3. Model Calibration Results.

Table 3. Temperature Boundary Conditions.

Surface	Temperature (K)
Piston	600
Liner	450
Intake valves	550
Exhaust valves	800
Intake port	350
Exhaust port	600
Cylinder head	500
Spark plug	900

3. Combustion Chamber Design Scheme

Four different types of combustion chambers with a constant compression ratio were designed, which are shown in Figure 4. The combustion chamber v1 increases the extrusion area to improve the incylinder extrusion, It is a type of constricted combustion chamber; Combustion chamber v2 is a shallow pit type combustion chamber with smaller bowl depth and increased compression height; Combustion chamber v3 adopts the highest compression height and a combustion chamber depth of 0, forming a flat top combustion chamber; The combustion chamber v4 maintaining a constant cylinder head surface is matched with a spherical bowl to assist in generating and maintaining rolling motion, which is closer to a typical spark ignition engine design.

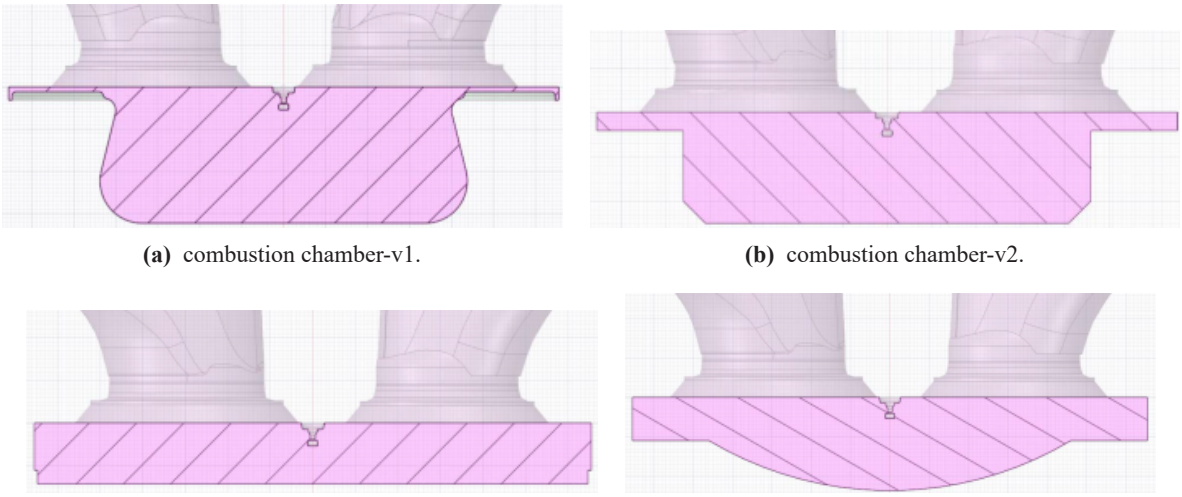

(a) combustion chamber-v1. **(b)** combustion chamber-v2.

(c) combustion chamber-v3. **(d)** combustion chamber-v4.

Figure 4. Combustion Chamber Design Scheme.

4. Calculation Results and Analysis

4.1. Flow Field and Turbulence Characteristics

Typically, three types of inflation motion characteristics are involved in the combustion chamber, namely: tumble flow (tumble number), vortex flow (vortex number), and turbulent kinetic energy (TKE). tumbling flow is the rotation of gas, with the axis of rotation perpendicular to the cylinder axis.

The tumble flow generation mainly depends on the design of the intake port, and the geometric structure of the cylinder head, including the cover, can also be used to enhance tumble flow during small valve lift. The formation and protection of tumble flow is ensured by the designed combustion chamber. Vortex is the rotation of gas, with its axis aligned with the cylinder axis. The contribution to the vortex mainly comes from the intake port design. For small valve lifts, valve seat chamfers can be used to enhance vortex motion, and combustion chamber design can support the formation and maintenance of a vortex. TKE indicates the degree of turbulence in the flow within a region. Usually, TKE is formed when large-scale eddies (rolling and vortices) decompose into small-scale structures. These small structures cannot be solved by the RANS turbulence model in this simulation model. On the other hand, TKE serves as a representative value to describe the energy contained in small-scale models. When the balance drops to the molecular level, they dissipate as heat. Generally speaking, TKE supports the propagation of flames. The initial laminar flame core was stretched and wrinkled by small scales. Therefore, the flame surface has been increased, and fuel consumption and flame speed have also increased.

4.1.1. Rolling Flow Motion

The calculation results of the rolling flow inside the cylinder are shown in Figure 5. Typically, two peaks are displayed on rolling curves. The first peak occurs during the intake stroke, when the combustion chamber is moving towards bottom dead center (BDC) and air is drawn into the combustion chamber at high

speed. The second peak occurs during the compression stroke with the upward movement of the combustion chamber. When the valve is closed and the combustion chamber volume decreases, there is a peak in momentum conservation in the captured fresh charge flow. The combustion chamber v1, with the highest value in the first roll peak, indicates its optimal charging motion during the intake stroke. The combustion chambers v2 and v4 perform excellently during the compression stroke, which is beneficial for generating TKE near spark timing and facilitating the flame progression after ignition.

For the combustion chamber v1, the absolute value of the cylinder tumble is 0.95 at the peak, relatively inferior to the most advanced passenger car SI engines, originating from a lack of a specific rolling air intake design. This occurs simultaneously with the unaffected intake design in this study.

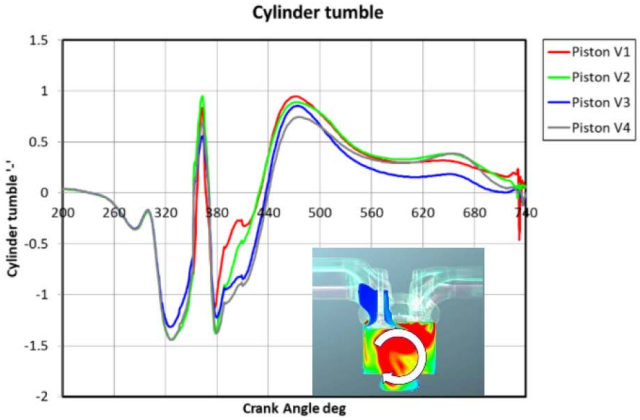

Figure 5. Calculation results of cylinder tumble.

4.1.2. Vortex Motion

The calculation results of the cylinder swirl number are shown in Figure 6. Swirl is mainly formed during the suction stroke. The combustion chamber v1, with the typical diesel combustion chamber design, has the highest vortex level among the analyzed geometries. As the depth of the bowl decreases, the vortex level also decreases, resulting in the minimum vortex of v3.

The swirl number level of the discussed combustion chamber is usually relatively low compared to the intake geometry. An improved intake geometry with a more tangential angle can be used to increase the vortex level.

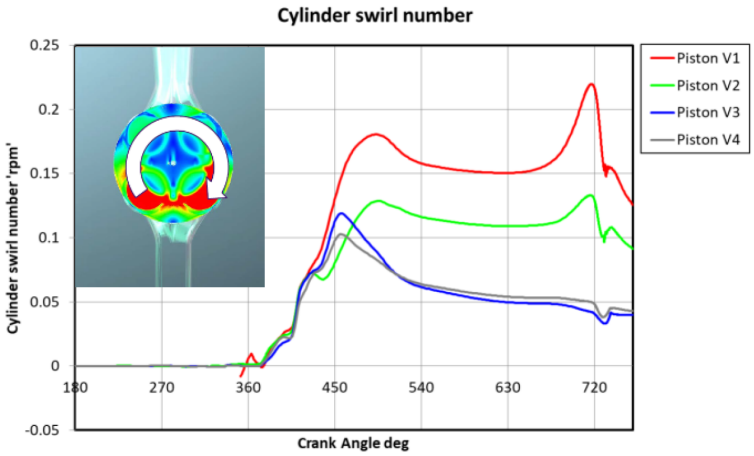

Figure 6. Calculation results of cylinder swirl number.

4.1.3. Turbulent Kinetic Energy

The calculation results of average turbulent kinetic energy inside the cylinder and around the spark plug are shown in Figures 7 and 8. The level of TKE near the cylinder and spark plug is exhibited the same along

TKE trajectories of the entire cycle for the four combustion chambers.

Notably, it can be seen that the combustion chamber v2 exhibits the highest TKE level at the end of the compression stroke, both inside the cylinder and near the spark timing spark plug.

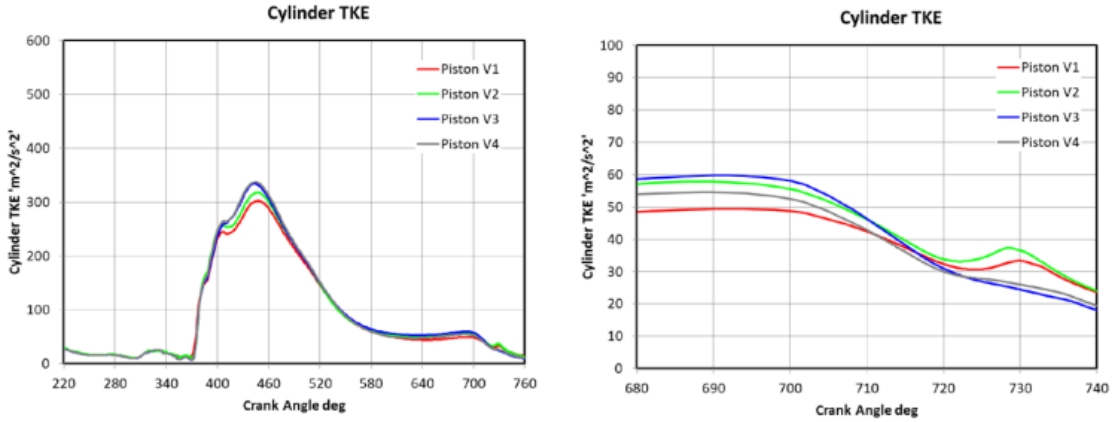

Figure 7. Calculation results of the average turbulent kinetic energy inside the cylinder.

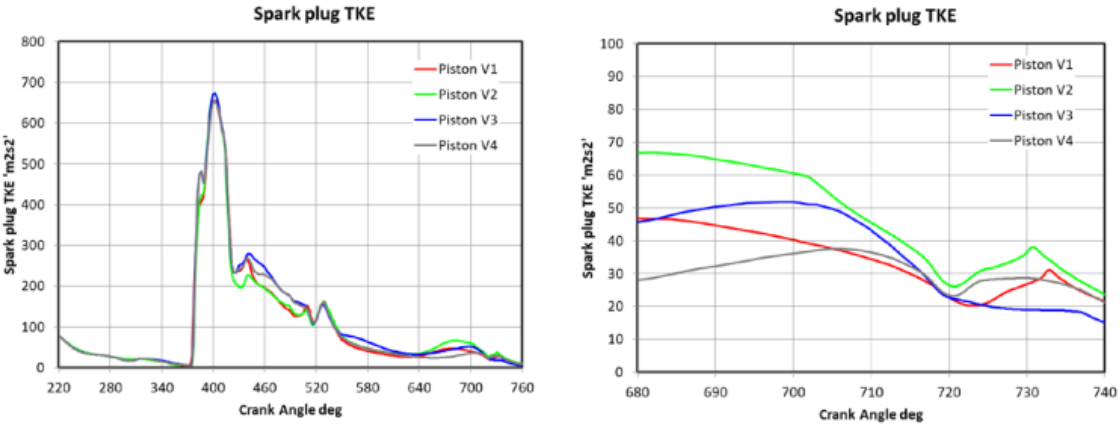

Figure 8. Calculation results of the average turbulent kinetic energy around the spark plug.

The distribution of turbulent energy inside the cylinder is shown in Figure 9. Higher TKE near the spark plug can facilitate early flame propagation after ignition. A higher TKE in the cylinder facilitates flame propagation through the combustion chamber. Observing the spatial distribution, a shorter distance between the high TKE regions of the combustion chamber scheme v2 can be surveyed. Indicating better combustion characteristics, i. e., faster flame propagation.

4.2. Combustion Characteristics Analysis

Cylinder combustion temperature, cumulative heat release rate, and in-cylinder pressure matter essentially for the combustion effect. In other words, stable and rapid release of heat is crucial. The impact of TKE and the combustion chamber on combustion is prominent based on the assumption that the air/fuel mixture is homogeneous in the study.

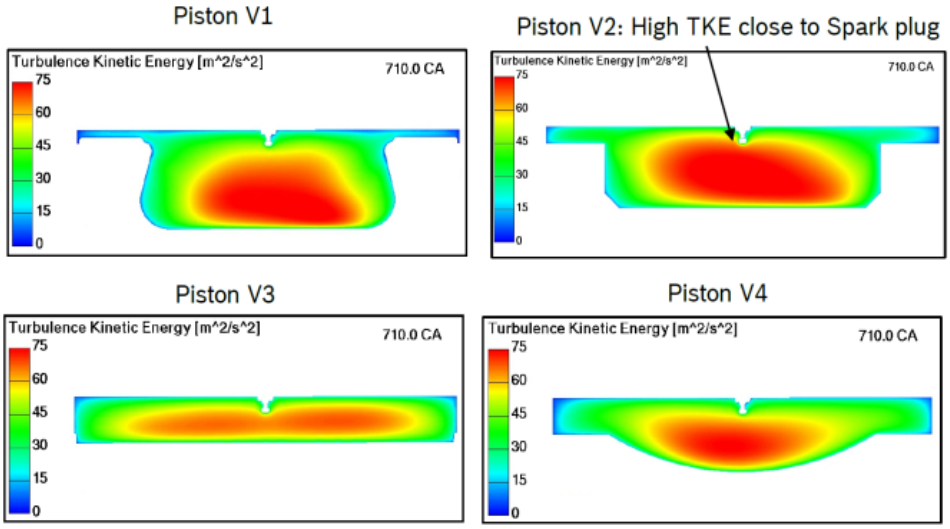

Figure 9. Distribution of turbulent energy in cylinder.

4.2.1. Combustion Temperature inside the Cylinder

The combustion temperature distribution of the cylinder under the combustion chambers is shown in Figure 10. All the combustion temperature inside the cylinder of the four combustion chambers reaches a maximum value of about 2500 K, achieving complete combustion. The varying rate of temperature rise is reflected due to the difference in heat release rate. The combustion chamber v2, featuring the fastest temperature rise rate, induces maximum temperature. In addition, the flame front, signified by combustion temperature, develops more rapidly in the longitudinal direction, covering the bottom surface of the combustion in a relatively short period. From the perspective of flame propagation, the symmetry of flame propagation and the overall combustion rate can be enhanced by increasing the depth of the combustion chamber appropriately.

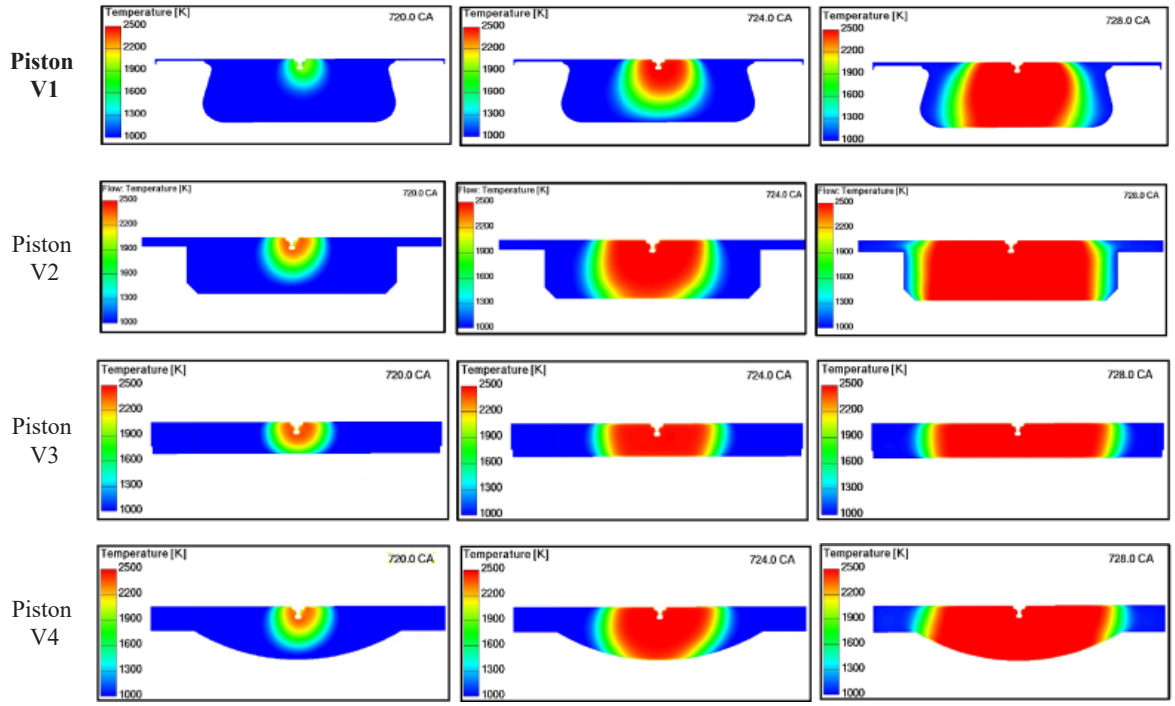

Figure 10. Distribution of combustion temperature inside the cylinder for combustion chambers.

4.3.2. Cumulative Heat Release Rate

The cumulative heat release rate calculation results are shown in Figure 11, and the combustion phase calculation results for combustion chambers are shown in Table 4. Fuel injected into the cylinder per cycle is 220 mg, releasing 11,000 joules of heat. According to the calculation results of the cumulative heat release rate, the heat release rate shows an ascending slope initially in the combustion chamber V1, but due to the large amount of flame/wall interaction in the compression zone, the heat release rate slows down near the end of combustion; Conversely, combustion chambers V3 and V4 possess faster heat release at the end of combustion, profiting from the increased compression height and reduced flame/wall interaction; In conclusion, the combustion chamber V2 facilitating the initial flame and the flame progression achieve the fastest heat release, benefiting from the highest TKE near the spark plug. Flame propagation after 70% heat release slows down, originating from the flame front developing difficulty in the squeezed area. Compared to the V1 design, the deceleration is reduced.

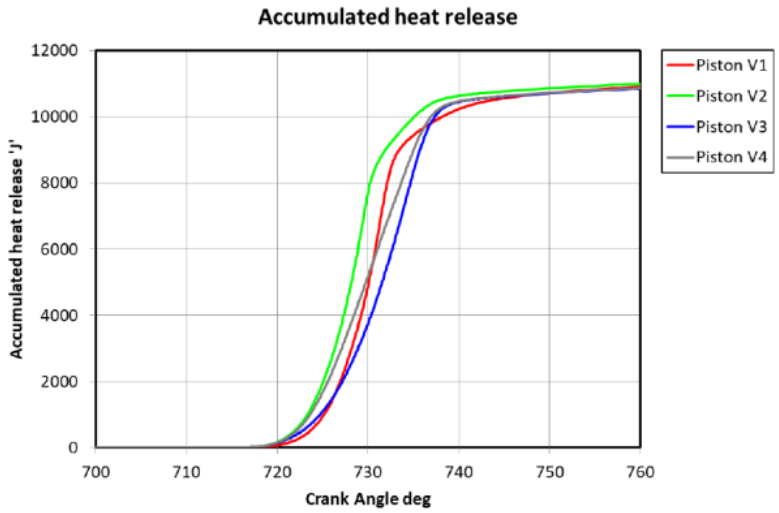

Figure 11. Calculation results of the cumulative heat release rate.

Table 4. Calculation results of the combustion phase for combustion chambers.

Combustion Chamber Scheme	B10 (°CA)	B50 (°CA)	B90 (°CA)
V1	725.4	730.5	737.6
V2	719.5	728.6	734.8
V3	725.1	732.2	737.2
V4	723.9	730.5	736.7

Therefore, ensuring a high TKE at the spark plug to achieve good flame initiation is essential for releasing heat more quickly, low flame wall interaction in the early stages of combustion achieves rapid heat release, and reasonable compression height advances the flame to the periphery of the cylinder.

4.3.3. Combustion Pressure inside the Cylinder

The calculation result of combustion pressure inside the cylinder is shown in Figure 12. It can be noticed that the cylinder pressure is almost the same in the compression stage for all combustion chambers. The pressure and temperature curves in combustion chambers V1 and V2 are parallel to each other after the spark, exhibiting similar combustion characteristics in both cases. However, flame initiation in combustion chamber v2 is better, resulting in faster heat release and higher peak pressure. Due to the insufficient flame propagation space mentioned above, the peak pressure of combustion chamber design V3 and combustion chamber design V4 decreases.

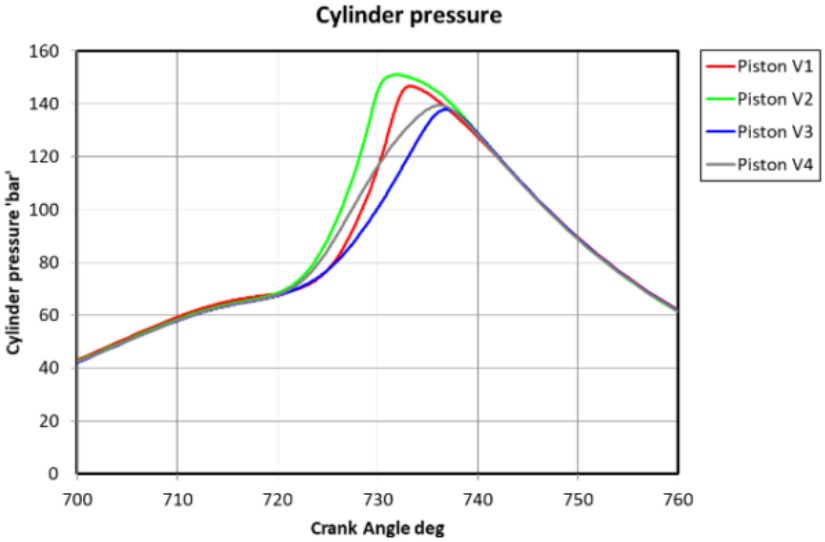

Figure 12. Calculation results of combustion pressure inside the cylinder.

5. Conclusions

Based on the optimization research summarized above, several conclusions can be drawn as follows:

(1) The comprehensive property of combustion chamber V2, featuring excellent flow characteristics, such as high TKE and tumble flow, is superior. The sufficient compression height for flame propagation also benefits a lot.

(2) Combustion chamber V1 with a diesel bowl-shaped design generates TKE and rolling flow near spark plugs insufficiently, resulting in inadequate flame formation. The low compression height hinders the flame propagation process towards the periphery of the combustion chamber.

(3) Combustion chamber V4 promotes the generation of rolling flow and TKE near the spark plug, accelerating the formation and development of flames. However, wall interaction retards flame propagation

(4) The balance between compression height and combustion chamber depth must be considered in combustion chamber design to optimize the fluid flow and combustion characteristics of the engine.

Numerous unresolved challenges still exist in heavy-duty natural gas engines, such as the reduction of hydrocarbon emissions, suppression of knock, and improvement of thermal efficiency. To address these challenges, a multi-factor collaborative optimization study based on automatic optimization algorithms will be further conducted on intake manifold structure, combustion chamber, ignition timing, and EGR rate, enhancing the overall performance and market potential of heavy-duty natural gas engines.

Author Contributions: H.C. and Z.L.: conceptualization, methodology, software; B.L.: data curation, writing—original draft preparation; H.Z. (Huiya Zhang): visualization, investigation; Q.Z.: supervision; F.G.: software, validation; H.Z. (Hongfei Zhang): writing—reviewing and editing. All authors have read and agreed to the published version of the manuscript.

Funding: This research received no external funding.

Informed Consent Statement: Informed consent was obtained from all subjects involved in the study.

Data Availability: Statement: Not applicable.

Conflicts of Interest: The authors declare no conflict of interest. The funders had no role in the design of the study; in the collection, analyses, or interpretation of data; in the writing of the manuscript; or in the decision to publish the results.

References

1. Kusaka, J.; Okamoto, T.; Daisho, Y.; Kihara, R.; Saito, T. Combustion and exhaust gas emission characteristics of a diesel engine dual-fueled with natural gas. *JSAE Rev.* **2000**, *21*, 489–496. https://doi.org/10.1016/S0389-4304(00)00071-0.
2. Zheng, Q. P. *Simulation Calculation and Experimental Study of the Combustion Process of Compression-Ignition Natural Gas Engine*; Tianjin University: Tianjin, China, 2006.

3. Goto, S.; Lee, D.; Shakal, J. Performance and Emissions of an LPG Lean-Burn Engine for Heavy Duty Vehicles. *SAE* **1999**, *108*, 1055–1065. https://doi.org/10.4271/1999-01-1513.
4. Gulcan, H.E.; Ciniviz, M. Experimental study on the effect of piston bowl geometry on the combustion performance and pollutant emissions of methane-diesel common rail dual-fuel engine. *Fuel* **2023**, *345*, 128175. https://doi.org/10.1016/j.fuel.2023.128175.
5. Bao, J.; Qu, P.; Wang, H.; Zhou, C.; Zhang, L.; Shi, C. Implementation of various bowl designs in an HPDI natural gas engine focused on performance and pollutant emissions. *Chemosphere* **2022**, *303*, 135275. https://doi. org/10.1016/j.chemosphere.2022.135275.
6. Xu, G.; García, A.; Jia, M.; Monsalve-Serrano J. Computational optimization of the piston bowl geometry for the different combustion regimes of the dual-mode dualfuel (DMDF) concept through an improved genetic algorithm. *Energy Convers. Manag.* **2021**, *246*, 114658. https://doi.org/10.1016/j.enconman.2021.114658.
7. Li, W.; Ma, J.; Liu, H.; Wang, H.; Zhang, H.; Qi, T.; Pan, J. Investigations on combustion system optimization of a heavy-duty natural gas engine. *Fuel* **2023**, *331*, 125621. https://doi.org/10.1016/j.fuel.2022.125621.
8. Wohlgemuth, S.; Roesler, S.; Wachtmeister, G. Piston design optimization for a twocylinder lean-burn natural gas engine-3D-CFD-simulation and test bed measurements. *SAE Tech. Paper* **2014**. https://doi.org/10.4271/2014-01-1326.
9. Raju, A.; Ramesh, A.; Nagalingam, B. Effect of intensiffed swirl and squish on the performance of a lean burn engine operated on LPG. *SAE Tech. Paper* **2000**. https://doi.org/10.4271/2000-01-1951.
10. Fu, X. *Study on the Interaction Mechanism between in-Cylinder Turbulence and Combustion of Natural Gas Engines*; Jilin University: Jilin, China, 2022.
11. Zhang, S.; Duan, X.; Liu, Y.; Guo, G.; Zeng, H.; Liu, J.; Yuan, Z. Experimental and numerical study the effect of combustion chamber shapes on combustion and emissions characteristics in a heavy-duty lean burn SI natural gas engine coupled with detail combustion mechanism. *Fuel* **2019**, *258*, 14. https://doi.org/10.1016/j. fuel.2019.116130.
12. Wang, S.; Li, Y.; Fu, J.; Liu, J.; Dong, H.; Tong, J. Quantitative investigation of the effects of EGR strategies on performance, cycle-to-cycle variations and emissions characteristics of a higher compression ratio and heavy-duty NGSI engine fueled with 99% methane content. *Fuel* **2020**, *263*, 14. https://doi.org/10.1016/j. fuel.2019.116736.
13. Liu, L.D.; Zhang, M.L.; Liu, Z.B. A Review of Development of Natural Gas Engines. *Int. J. Automot. Manuf. Mater.* **2023**, *2*, 4. https://doi.org/10.53941/ijamm0201004.
14. Lu, C.; Chen, W.; Zuo, Q.; Zhu, G.; Zhang, Y.; Liu, Z. Review of Combustion Performance Improvement and Nitrogen-Containing Pollutant Control in the Pure Hydrogen Internal Combustion Engine. *Int. J. Automot. Manuf. Mater.* **2022**, *1*, 7. https://doi.org/10.53941/ijamm0101007.
15. Gao, Y.; Huang, W.; Pratama, R. H.; Wang, J. Transient Nozzle-Exit Velocity Profile in Diesel Spray and Its Influencing Parameters. *Int. J. Automot. Manuf. Mater.* **2022**, *1*, 8. https://doi.org/10.53941/ijamm0101008.
16. Bao, L.; Wang, J.; Shi, L.; Chen, H. Exhaust Gas After-Treatment Systems for Gasoline and Diesel Vehicles. *Int. J. Automot. Manuf. Mater.* **2022**, *1*, 9. https://doi.org/10.53941/ijamm0101009.
17. Yu, X.; Jin, Y.; Liu, H.; Rai, A.; Kostin, M.; Chantzis, D.; Politis, D.J.; Wang, L. A Review of Renewable Energy and Storage Technologies for Automotive Applications. *Int. J. Automot. Manuf. Mater.* **2022**, *1*, 10. https://doi. org/10.53941/ijamm0101010.